Biomolecules and Biomedicine
ISSN: 2831-0896 (Print) | ISSN: 2831-090X (Online)
Journal Impact Factor® (2024): 2.2
CiteScore® (2024): 5.2
www.biomolbiomed.com | blog.bjbms.org

RESEARCH ARTICLE

Ashraf et al: Rifaximin–berberine synergy in KP

Synergistic effect of the rifaximin–berberine combination against *Klebsiella pneumoniae*: RfaH targeting supported by MD simulation

Anam Ashraf[1#], Mohammad Ali Khan[2#], Arunabh Choudhury[1], Swati Kumari[3], Bader S. Alotaibi[4], Saba Noor[1], Mohd Adnan[5], Md. Imtaiyaz Hassan[1*]

[1]Centre for Interdisciplinary Research in Basic Sciences, Jamia Millia Islamia, New Delhi, India;

[2]Department of Biotechnology, School of Chemical and Life Sciences, Jamia Hamdard, New Delhi, India;

[3]National Institute of Immunology, New Delhi, India;

[4]Department of Clinical Laboratory Sciences, College of Applied Medical Sciences, Shaqra University, Al-Quwayiyah, Riyadh, Saudi Arabia;

[5]Department of Biology, College of Science, University of Ha'il, Ha'il, Saudi Arabia.

[#]Equally contributed to this work: Anam Ashraf and Mohammad Ali Khan.

*Correspondence to Md. Imtaiyaz Hassan: mihassan@jmi.ac.in

DOI: https://doi.org/10.17305/bb.2026.13776

ABSTRACT

The escalating crisis of antimicrobial resistance (AMR) among Gram-negative pathogens, particularly *Klebsiella pneumoniae* (KP), necessitates innovative strategies to enhance the efficacy of existing antibiotics. Synergistic drug combinations present a promising approach to improve therapeutic outcomes and delay the emergence of resistance. This study investigates the synergistic interaction between the natural alkaloid berberine chloride and the repurposed antibiotic rifaximin against KP. Integrated *in vitro* and *in silico* analyses reveal significant bactericidal synergy between the two agents, mediated through concurrent inhibition of the transcriptional anti-termination factor RfaH, a key regulator of virulence and capsule biosynthesis. Molecular docking and dynamics simulations demonstrate that both compounds cooperatively bind to the RfaH pocket, stabilizing an inactive ternary complex without major structural disruption. Functional assays confirm that the combination effectively suppresses RfaH-dependent capsule production at lower concentrations compared to monotherapy. These findings suggest that RfaH is a viable target for combinatorial inhibition and provide a plausible mechanistic foundation for the berberine–rifaximin synergy. This work supports the rational development of dual-targeting anti-virulence strategies to combat multidrug-resistant KP infections.

Keywords: Synergistic effect, rifaximin-berberine, anti-termination protein RFAH, MD simulation, antibiotic resistance, *K. pnuemoniae.*

INTRODUCTION

Klebsiella pneumoniae (KP) is a key opportunistic pathogen within the Enterobacteriaceae family. It is not a single homogeneous entity but encompasses distinct and concerning clinical phenotypes. It causes a broad spectrum of diseases while demonstrating a concerning trend of escalating antibiotic resistance (1). These include classical multidrug-resistant (MDR) strains, hypervirulent (hvKp) strains associated with severe community-acquired infections, and increasingly prevalent hybrid isolates that combine hypervirulence with multidrug-resistance traits, posing a dual threat to public health (2, 3). In the WHO bacterial priority pathogens list (2024), carbapenem-resistant KP was ranked as the top-priority pathogen with a total score of 84%, placing antibiotic-resistant KP strains in the highest quartile (4).

In Europe alone, KP is responsible for over 90,000 infections and approximately 7,000 deaths annually, accounting for a substantial 25% of the disability-adjusted life years lost to bacterial infections. The clinical management of these infections is severely complicated by the rising prevalence of multidrug-resistant strains, particularly those producing extended-spectrum β-lactamases (ESBLs) and carbapenemases. This resistance profile often forces a reliance on last-line treatments like colistin in combination with β-lactamase inhibitors, which are suboptimal due to potential toxicity and variable efficacy (5). A major factor complicating the prevention of these infections is the current absence of any efficient and licensed vaccination strategy, despite extensive ongoing research efforts (6). Infections caused by drug-resistant KP represent a grave public health threat. The continuous evolution and rising multidrug resistance of KP pose a direct risk to humans (7).

The transcriptional elongation factor RfaH facilitates expression of long virulence operons in various bacteria. Its role in KP is essential, promoting capsular polysaccharide (CPS) synthesis, hypermucoviscosity, and overall bacterial fitness during infection (8). Deleting *rfaH* significantly attenuated virulence in KP NTUH-K2044, which is a highly virulent, hypermucoviscous K1 serotype reference strain causing liver abscesses and meningitis (9). The impairment of LPS biosynthesis due to *rfaH* deletion disturbs the proper assembly of outer membrane proteins. This disrupts the assembly of outer membrane proteins and thereby reduces membrane permeability (10). Under iron restriction, the *rfaH* mutant exhibits reduced growth kinetics, primarily attributed to deficient CPS production. This attribution is supported

by the established correlation between CPS biosynthesis and iron availability in hypervirulent KP (hvKp). Impaired RfaH-regulated CPS synthesis likely disrupts physiological adaptations essential for efficient growth (11). These findings position RfaH as a novel and attractive target for the development of anti-infective strategies against KP.

With antibiotic discovery rates drastically declining despite pharmaceutical initiatives, the WHO urgently calls for novel therapies. Plant natural products (NPs) offer a strategic solution, drawing on their historical significance as sources of bioactive agents and ethnopharmacological knowledge (12-14). *Coptis chinensis* Franch is a pharmacopoeial herb and also known as Huanglian in Traditional Chinese Medicine (TCM). Extracts derived from *C. chinensis* exhibit potent, broad-spectrum antibacterial activity for the management of conditions such as dysentery, cholera, leukemia, diabetes, and lung cancer. The primary constituents responsible for the observed pharmacological effects, particularly the antimicrobial properties, are isoquinoline alkaloids, with berberine representing the major bioactive component (15).

A study has shown that berberine has potent *in vitro* antimicrobial activity against methicillin-resistant *Staphylococcus aureus* (MRSA), with promisingly low minimum inhibitory concentration values (16). Berberine has demonstrated antimicrobial efficacy in both traditional and modern medicine. In recent research, the berberine core was modified to yield a series of novel Schiff base analogues as a scaffold for the development of antimicrobial agents.

The potential of these berberine-derived compounds was evaluated and has shown enhanced antimicrobial activity against *Pseudomonas aeruginosa*, *Aspergillus fumigatus, Staphylococcus epidermidis,* and *Candida albicans* by free radical scavenging assays (17). Building upon studies highlighting the significant potential of berberine as a novel antimicrobial agent and supporting our prior work demonstrating the successful repurposing of rifaximin to target RfaH in KP (18, 19).

This study investigates the synergistic potential of berberine and rifaximin against this pathogen. Given the substantial challenges in discovering entirely new drugs for multidrug-resistant infections such as KP, exploring synergistic combinations of existing or repurposed compounds is a promising, time-efficient strategy. We

employed integrated *in silico* (molecular docking and molecular simulation analysis) and *in vitro* (checkerboard assays, time-kill curves) techniques to rigorously evaluate the interaction between berberine and rifaximin, aiming to identify potent combination therapies that could expedite therapeutic development.

MATERIALS AND METHODS

Materials

Rifaximin, berberine chloride, and ciprofloxacin were purchased from Sigma-Aldrich (St. Louis, MO, USA). Luria Bertini broth and Nutrient Agar were obtained from HiMedia Laboratories (Maharashtra, India). p-Iodonitrotetrazolium chloride (INT) was purchased from Merck (Darmstadt, Germany). BIOMOL® Green reagent was procured from Enzo Life Sciences (New York, USA). All other chemicals and solvents were of analytical grade.

Fluorescence measurements

To evaluate the binding affinity of RfaH for rifaximin, berberine chloride, and their combination, a fluorescence-quenching study was performed using a Jasco FP-8200 spectrofluorometer (Japan). The stock solutions of both compounds were prepared in DMSO at 50 mM, then diluted into Tris-NaCl buffer (50 mM Tris-HCl, 150 mM NaCl, pH 7.5) to a final working concentration of 0.5 mM. Throughout the experimental runs, the RfaH concentration was kept constant at 8.0 µM.

For experiments evaluating individual interactions, rifaximin and berberine chloride were each titrated into the RfaH solution at a 1:9 ratio, with additions continuing until no further quenching was observed. In the combination assays, both compounds were pre-mixed in a ratio of 50 µM rifaximin to 6.25 µM berberine chloride (8:1 molar ratio), corresponding to the synergistic concentrations identified in microbiological assays. This mixture was then titrated into the RfaH solution using the same titration procedure. Fluorescence emission was recorded over 300-400 nm, with excitation set to 280 nm to target tryptophan residues. Slit widths and sensitivity settings were maintained for all spectral parameters to ensure data consistency. Fluorescence quenching parameters were evaluated using a modified Stern–Volmer relationship to determine the binding constant (*K*a) and the number of binding sites (*n*) for each test condition: rifaximin alone, berberine chloride alone, and their equimolar mixture. All

experiments were conducted in triplicate, and corrections were applied to remove background fluorescence from the buffer and potential inner-filter effects. By integrating these steps into the workflow, we characterized the interaction of RfaH with the individual compounds and their combination with high accuracy and reproducibility, using our well-established protocols (20-22).

Minimum inhibitory concentration measurements

The bacterial strain used was KP ATCC 700603. This strain, widely utilized as an ESBL-producing reference strain, is phylogenetically classified within *Klebsiella quasipneumoniae subsp. similipneumoniae*. For consistency with the ATCC designation and common literature references, we refer to it herein as KP ATCC 700603. To assess antibacterial strength, the minimum inhibitory concentrations (MICs) of rifaximin, berberine chloride, and their combined formulation were determined against KP (ATCC 700603) using a p-iodonitrotetrazolium chloride (INT) based colorimetric assay. Each compound was initially dissolved in DMSO, with the solvent concentration carefully limited to below 2.5% in the final mixtures to avoid any negative impact on bacterial viability. For single-agent testing, serial two-fold dilutions were prepared in broth across the rows of a 96-well microtiter plate, with final concentrations ranging from 200 µM to 0.78 µM. Wells were inoculated with 100 µL of bacterial suspension (~1.5×10^5 CFU/mL). For the combination study, the checkerboard method described below was employed.

Checkerboard assay

To examine potential drug–drug interactions, a checkerboard microdilution method was applied. Rifaximin was serially diluted two-fold along the rows (final concentration range: 100 µM to 0.78 µM), while berberine chloride was diluted similarly down the columns (final concentration range: 100 µM to 0.78 µM). Each well thus contained a unique combination of both agents. Wells of the assay plate were inoculated with 100 µL of bacterial suspension KP (ATCC 700603, approximately 1.5×10^5 CFU/mL) and incubated at 37 °C for 18 hours. Following this period, INT dye was added to obtain a final concentration of 0.2 mg/mL, and the plates were left for a further 30 minutes under the same conditions. The reduction of yellow INT to pink hue indicated active bacterial metabolism. The MIC for each well was defined as the lowest concentration at which the dye retained its original yellow

color, indicating complete inhibition of bacterial growth. Control groups comprised wells containing only bacterial cultures without any drug exposure, as well as wells with sterile medium to assess background signals. Ciprofloxacin-treated wells served as the control for growth inhibition. Each assay was conducted in triplicate to confirm reproducibility. In experiments involving both rifaximin and berberine chloride, the fractional inhibitory concentration index (FICI) was calculated to quantify their interaction and distinguish between synergistic, additive, or antagonistic effects (23).

The FICI was calculated using the equation:

FICI = (MIC_A in combination / MIC_A alone) + (MIC_B in combination / MIC_B alone)

Where MIC_A and MIC_B represent the minimum inhibitory concentrations of rifaximin and berberine chloride, respectively, determined alone or in combination.

Determination of minimum bactericidal concentration

Time-kill assays were performed to investigate the bactericidal effects of rifaximin, berberine chloride, and their combined treatment against KP (ATCC 700603). Bacterial cells in the early logarithmic phase were exposed to each agent alone and in combination at concentrations equal to their respective MICs. For combination testing, the drug concentrations were selected based on the synergistic ratios determined in the prior checkerboard assay. Samples were collected at 0, 3, 6, 9, and 24 hours, serially diluted, and plated onto nutrient agar to count viable colonies after 24 hours of incubation. Two sets of controls were comprised: untreated bacterial cultures as the growth control, and sterile medium to verify sterile conditions. CFU counts were graphed on a logarithmic scale (y-axis) against time (x-axis) to determine bactericidal dynamics. All experiments were performed in triplicate to ensure reproducibility. This approach enabled direct evaluation of the time-dependent bactericidal activity of rifaximin, berberine chloride, and their combined treatment against KP (24). All experiments were performed in triplicate to ensure reproducibility. Synergy in time-kill assays was defined as a ≥ 2 $\log_{10}$ CFU/mL decrease in viable count by the combination compared to the most effective single agent at the same time point (25).

Capsule quantification assay

Capsular polysaccharide (CPS) synthesis and uronic acid content of KP (ATCC 700603) were evaluated using a capsule quantification method adapted from previously reported methods (26, 27). Cultures grown in 20 mL LB broth were incubated for 16 hours under four conditions: 100 µM rifaximin, 100 µM berberine chloride, a combination of both, or no treatment (control). For combination treatment, cultures were exposed to 50 µM rifaximin and 6.25 µM berberine chloride simultaneously. Bacterial concentrations were standardized based on CFU/mL counts before CPS extraction. Extraction of CPS followed a modified Zwittergent-based method (28), in which 500 µL of culture was combined with 1% Zwittergent in 100 mM citric acid, incubated at 50 °C for 20 minutes, and afterward centrifuged at 10,000 × g for 5 minutes. Supernatants were precipitated with cold ethanol at 4°C for 20 minutes, and pellets were resuspended in distilled water. Uronic acid content was measured by reacting to the samples with 12.5 mM sodium tetraborate in concentrated sulfuric acid, followed by heating at 95 °C for 5 minutes. Subsequently, 0.15% 3-phenylphenol prepared in 0.5% sodium hydroxide was added to initiate color formation. The absorbance at 520 nm was recorded and adjusted for bacterial concentration (CFU/mL) to determine relative CPS levels. Each assay was performed in triplicate, allowing consistent and reliable assessment of CPS yield and uronic acid concentration in rifaximin-, berberine-, and combination-treated cultures relative to untreated controls.

Molecular docking

We have performed molecular docking of RfaH against rifaximin and berberine chloride. The RfaH structure was obtained from the AlphaFold database (ID: AF-A0A2X3CVV5-F1-model_v4). The molecular docking, ligand preparation, protein preparation, and grid preparation were performed using InstaDock (29). A grid box with coordinates X: –4.482, Y: –1.653, Z: 0.019 and the dimensions of 64 Å, 58 Å, and 78 Å for the X, Y, and Z axes, respectively. Following docking, interaction analysis was performed to identify the best docked conformation using PyMOL (30).

Molecular dynamics simulation

All-atom molecular dynamics (MD) simulations were carried out to assess the stability and efficiency of protein-ligand interactions (31, 32). The simulations were

performed using GROMACS 2022.2 (33) with the CHARMM36 (34) force field for free RfaH, and RfaH-rifaximin, RfaH-berberine chloride, RfaH-(rifaximin + berberine chloride) complexes. Ligand topologies were generated using the CGenFF web server, and explicit hydrogen atoms were added to the structures in Avogadro before simulation. Each protein and its protein–ligand complex was placed in a cubic simulation box with an edge length of 10 Å. The systems were solvated using the TIP3P water model, and neutralization was performed by adding appropriate counterions. Equilibration was carried out in two stages: first under constant-volume (NVT) conditions, followed by constant-pressure (NPT) conditions. The temperature was maintained at 300 K with a coupling time constant of 0.1 ps. A 200 ns production run was then executed for each system. The resulting trajectories were analyzed using the built-in GROMACS tools to evaluate the dynamic behavior and overall stability of the protein–ligand complexes.

RESULTS

Drug repurposing, exemplified by the FDA approval of favipiravir for influenza (35) and Closantel for antibiotic-resistant (VRSA strain VRS1) *Staphylococcus aureus* infections (36), offers a promising strategy to rapidly address KP infections. Building on this concept, our prior research established rifaximin, which is a non-systemic gut-targeted antibiotic, as a repurposed candidate against KP by demonstrating its interaction with the transcriptional elongation factor RfaH. Driven by the urgent need for effective anti-KP therapies and leveraging the repurposing potential of rifaximin, this study evaluated the synergistic antibacterial activity of rifaximin combined with berberine chloride. Berberine chloride is a natural isoquinoline alkaloid with established broad-spectrum antimicrobial properties, aimed at enhancing therapeutic efficacy against this challenging pathogen.

Antibacterial activity of berberine chloride in combination with the antibiotic rifaximin against KP

The antibacterial efficacy of rifaximin and berberine chloride KP ATCC 700603 was quantitatively assessed using the INT colorimetric assay to determine MIC. Individually, both agents demonstrated equivalent intrinsic activity, with MICs of 100 μM. This rifaximin result aligns with our prior investigations (18). Strikingly, co-administration of the compounds using a checkerboard assay revealed a substantial

synergistic enhancement of antibacterial potency. The MIC for rifaximin decreased 2-fold to 50 µM, while the MIC of berberine chloride showed a pronounced 16-fold reduction to 6.25 µM. The checkerboard assay **(Supplementary Table 1)** revealed that the combination significantly reduced the effective concentration of both agents. The MIC of rifaximin decreased from 100 µM to 50 µM, and the MIC of berberine chloride decreased from 100 µM to 6.25 µM due to enhanced combinatorial activity. The Fractional Inhibitory Concentration Index (FICI) was calculated as follows: (50/100) + (6.25/100) = 0.5 + 0.0625 = 0.5625. An FICI of 0.56 indicates a partially synergistic interaction.

Time-kill assays provided strong evidence of bactericidal synergy, defined as a ≥2 $\log_{10}$ CFU/mL decrease by the combination compared to the most effective single agent at the same time point (25). At 24 hours, the combination of 50 µM rifaximin and 6.25 µM berberine chloride achieved a 2.56 $\log_{10}$ CFU/mL reduction from the starting inoculum, which was greater than the 1.59 log reduction achieved by rifaximin alone (difference ≈ 0.98 $\log_{10}$) **(Figure 1, Supplementary Table 2).** However, this difference did not meet the predefined threshold for time-kill synergy (≥2 $\log_{10}$ decrease compared to the most effective single agent). Time-kill assays demonstrated enhanced bactericidal activity of the combination compared to either agent alone. Collectively, these findings, spanning MIC reduction, FICI, and dynamic kill curves, establish a compelling foundation for rifaximin in combination with berberine chloride as a promising therapeutic strategy against multidrug-resistant KP infections.

Synergistic enhancement of RfaH binding revealed by intrinsic fluorescence quenching

Intrinsic fluorescence spectroscopy was employed to characterize the molecular interactions of rifaximin, berberine chloride, and their combination with the RfaH protein. Ligand-induced perturbations to the local environment of aromatic residues, such as tryptophan, tyrosine, and phenylalanine, were monitored via changes in fluorescence emission.

Individual titration experiments demonstrated concentration-dependent quenching of RfaH fluorescence by both compounds, consistent with direct binding **(Figure 2A**

and 2C). Analysis using a modified Stern-Volmer equation revealed that rifaximin bound RfaH with high affinity ($K_a = 7.38 \times 10^6\ M^{-1}$), as shown in our prior study (18). Berberine chloride exhibited moderate binding affinity, depicting a K_a value of $1.09 \times 10^6\ M^{-1}$ **(Figure 2B and 2D)**. Critically, when combined with a fixed concentration of rifaximin and a reduced concentration of berberine chloride, the co-treatment induced synergistic fluorescence quenching **(Figure 2E).** This combination elicited a significant quenching response. Fitting the experimental data revealed an enhanced binding affinity of $6.86 \times 10^7\ M^{-1}$, representing an almost 10-fold increase over the affinity observed for rifaximin and berberine alone **(Figure 2F and Table 1).**

This enhancement in K_a signifies cooperative binding or ligand-induced conformational optimization of RfaH when both compounds are present. The observation that halving the concentration of berberine relative to its solo efficacy within the combination not only maintained but significantly amplified RfaH engagement aligns with established fluorescence signatures of combinatorial additive molecular interactions.

Effect of synergy on capsule production in KP

Capsule quantification assays performed on KP ATCC 700603 revealed distinct and comparative impacts of rifaximin, berberine chloride, and their combination on capsule production. Treatment with rifaximin alone at 100 µM, a concentration previously shown to be effective, induced a significant reduction in capsule production, exceeding 50% relative to the untreated control, thereby confirming prior observations. Administration of berberine chloride at its inhibitory concentration resulted in a milder effect, decreasing capsule content by approximately 30%. Notably, co-administration of rifaximin and berberine chloride at lower concentrations (50 µM and 6.25 µM, respectively) produced a synergistic reduction in capsule biosynthesis **(Figure 3)**. This combination achieved a decrease comparable to that of 100 µM rifaximin alone (approximately 50% reduction), despite using only half the rifaximin concentration required to achieve this level of suppression when used as a single agent at its MIC-equivalent efficacy.

Rifaximin-berberine combination achieves synergistic capsule suppression through a concerted, two-way attack on RfaH. Rifaximin provides direct, competitive inhibition

at the functional interface, while berberine induces dysregulation via allosteric trapping. Their binding is cooperative, leading to a stabilized, inactive ternary complex that effectively halts the transcriptional program essential for capsule biosynthesis. This elegant mechanistic understanding validates RfaH as a viable target for combinatorial antimicrobial therapy. It provides a rational basis for employing dual-targeting strategies to combat resilient pathogens such as KP.

Interaction analysis of rifaximin and berberine chloride binding to RfaH

Molecular docking revealed rifaximin and berberine chloride bind to the RfaH protein with calculated binding affinities of -9.3 kcal/mol and -7.3 kcal/mol, respectively. An in-depth analysis of all nine docked conformations for each ligand was conducted to characterize their interactions within the RfaH binding pocket. Rifaximin forms hydrogen bonds with critical RfaH residues Tyr54 (β' clamp helices (CH) domain, 3.2 Å), Phe78 (3.0 Å), Arg80 (2.3 Å), and Asp147 (3.5 Å). Crucially, Tyr54 is a universally essential contact point for RfaH function, as literature studies demonstrate that disrupting interactions with β'CH (Tyr54), ops DNA (Arg73), β gate loop (βGL, Thr66), and S10 (Ile146) impairs RfaH-dependent gene activation in both *E. coli* and *KP* (28). Disruption of Tyr54 by rifaximin binding is therefore predicted to directly inhibit RfaH activity by interfering with this key functional interface. Rifaximin also engages in hydrophobic interactions with Tyr8 (3.93 Å), Val79 (3.73 Å), and Leu143 (3.86 Å). Visualization of the binding mode **(Figure 4A-C)** confirms rifaximin binds deeply within a pocket in RfaH, interacting specifically with residues of the β' CH domain.

In contrast, berberine chloride primarily targets the hydrophobic patch within the N-terminal domain (NTD), forming hydrogen bonds with Gly81 (3.3 Å) and Thr86 (3.5 Å). This patch is essential for stabilizing the autoinhibited α-helical state via interactions with the C-terminal domain (βCTD). Ligands or mutations disrupting this hydrophobic surface prevent the formation or maintenance of the autoinhibitory NTD-βCTD interface, rendering RfaH unable to adopt its inactive conformation (37). Critically, this patch is also necessary for initiating βCTD refolding back into the α-state after RfaH dissociates from the Transcription Elongation Complex (TEC). Consequently, berberine chloride binding to this patch is predicted to impair post-TEC refolding, effectively trapping RfaH in its active β-barrel conformation (β-state).

This locked active state leads to constitutive, dysregulated RfaH activity, resulting in aberrantly high-level translation of RfaH-dependent operons (e.g., virulence factors, capsule synthesis proteins), causing toxic overexpression, energetic waste, loss of coordinated gene regulation, and compromised cellular fitness or pathogenicity due to loss of temporal control (38). Berberine Chloride binds within the NTD hydrophobic patch cavity **(Figures 4A and 4B)** and penetrates deeply into the RfaH pocket **(Figure 4C),** like rifaximin.

Thus, while rifaximin inhibits RfaH by disrupting a critical functional contact point (Tyr54) within the β'CH domain, berberine chloride dysregulates RfaH by binding the NTD hydrophobic patch, preventing autoinhibition and trapping the protein in a constitutively active state. Both mechanisms exploit key interaction sites that have been demonstrated to be essential for RfaH function across bacterial species.

Structural dynamics and stability analysis of RfaH in complex with rifaximin and berberine chloride

Molecular dynamics simulations of RfaH, both in its native state and in complex with rifaximin, berberine chloride, or both ligands, provide significant insights into structural dynamics and stability by analyzing RMSD, *R*g, SASA, and RMSF. The native RfaH showed an average RMSD of 0.41 nm. When ligands bind individually, RMSD increased to 0.57 nm with rifaximin and 0.67 nm with berberine chloride, indicating reduced stability upon binding. When both ligands bind simultaneously, the RMSD decreased significantly to 0.36 nm, which is close to the native state. This decrease suggests that the synergistic ligand binding enhances the overall structural stability of RfaH **(Figure 5A).**

RMSF quantifies the flexibility of individual residues in a protein by measuring the average deviation of each residue's position over time relative to its mean position. The average for native RfaH was 0.24 nm. The rifaximin-bound complex shows an average RMSF of 0.30 nm, and the berberine chloride-bound complex shows 0.28 nm, indicating increased residue flexibility upon individual ligand binding. In contrast, the synergistic complex exhibited a reduced average RMSF of 0.21 nm. This decrease suggests that the synergistic binding of both ligands stabilizes specific residues,

effectively reducing their flexibility relative to the unbound and single-ligand states **(Figure 5B).**

Analysis of compactness via the radius of gyration (*R*g) revealed minimal variation across states. The native RfaH protein exhibited an average Rg of 1.78 nm, while the ligand-bound complexes with rifaximin and berberine chloride showed *R*g of 1.79, respectively. The synergistic complex showed an average *R*g of 1.79 nm. These small differences (Rg) suggest that ligand binding does not affect the global compactness of RfaH, maintaining the protein in a stable, compact conformation throughout the simulations **(Figure 6A).**

Solvent-accessible surface area (SASA) analysis indicated moderate structural rearrangements. Native RfaH had a SASA of 109.64 nm². Single ligand binding increased SASA (rifaximin: 114.12 nm²; berberine: 113.92 nm²). Crucially, dual ligand binding reduced SASA to 110.95 nm², closely resembling the native value. This SASA similarity between the native and synergistic bound states suggests minimal structural disruption upon dual ligand binding **(Figure 6B).**

Hydrogen bonds are justifiably termed the 'master key of molecular interactions' due to their ubiquity and flexibility, critically mediating biological processes such as ligand binding and enzyme catalysis (39). Hydrogen bonding analysis, encompassing both intra- and intermolecular interactions, was conducted to assess the stability of RfaH complexes. Evaluation of intramolecular hydrogen bonds within the RfaH structure over the 200 ns simulation duration revealed no significant alterations upon binding rifaximin, berberine chloride, or both ligands simultaneously compared to the native state.

The intermolecular hydrogen bond analysis showed the formation of up to four hydrogen bonds for the RfaH-berberine chloride complex, with one hydrogen bond remaining consistent **(Figure 7A).** Similarly, the RfaH-rifaximin plots showed the formation of up to 4 hydrogen bonds, with an average of 1 **(Figure 7B)**. On the other hand, the synergetic complex also forms four hydrogen bonds, with two remaining consistent throughout the simulation **(Figure 7C)**. The PDF plots showed the highest peak at 1 for the RfaH complexes with berberine chloride and rifaximin. In contrast,

the synergistic complex showed the largest peak at 2**,** indicating that complex formation does not perturb the protein's internal hydrogen-bonding network.

Collective analysis of RMSD, Rg, SASA, and RMSF highlights the stabilizing effects of ligand binding on RfaH. Reduced global flexibility (lower RMSD and RMSF values), maintained compactness (Rg), and altered solvent exposure (SASA) suggest structural adjustments that improve the enzyme's conformation for ligand binding (Table 2). These results offer valuable mechanistic insights into RfaH's functional behavior, aiding the rational design of effective inhibitors or modulators.

Secondary structure dynamics of native RfaH and synergistic complex

Analysis of secondary structure dynamics provides critical insights into protein conformational behavior and folding stability (40). Molecular dynamics simulations revealed that unbound RfaH maintains stable and equilibrated secondary structural elements throughout the 200 ns trajectory **(Figure 8A)**. The rifaximin-bound complex also showed preserved secondary structure topology, indicating that binding does not induce significant unfolding or destabilization of the protein fold **(Figure 8B).** Upon binding to berberine chloride, RfaH exhibited a similarly stable profile, with no major disruption to its core α-helical or β-sheet architectures **(Figure 8C).** The formation of the synergistic dual-ligand complex (RfaH-rifaximin-berberine) was accompanied by subtle conformational adjustments, characterized by a minor decrease in β-sheet content and a slight increase in α-helical structure **(Figure 8B)**. Quantification of residues engaged in regular secondary structures **(Table 3)** confirmed variations across all ligand-bound states (rifaximin, berberine, and dual-ligand complex) compared to the apo protein RfaH. Crucially, despite these measurable differences, the overall secondary structure topology of RfaH remains largely unaltered upon binding rifaximin alone, demonstrating the robust structural integrity of this complex.

Principal component analysis and free energy landscape

Principal component analysis (PCA) is a valuable computational technique for investigating protein conformational dynamics and collective atomic motions (41). In this study, PCA was employed to examine the conformational space explored by

RfaH in its unbound state and when complexed with rifaximin, berberine chloride, and the dual-ligand combination of rifaximin and berberine chloride. The analysis was performed using conformational projections based on the C^{α} atoms of RfaH to assess structural variations before and after ligand binding **(Figure 9).** The study showed that the RfaH-ligand complex occupied a more confined conformational subspace than the free protein, as well as the RfaH-rifaximin and RfaH-berberine chloride complexes. This suggested that binding the synergistic dual ligand increased the protein's stability while occupying its binding cavity.

Free energy landscapes are crucial for analyzing protein folding kinetics and thermodynamic parameters. Using the MD simulation trajectories, FELs provide insights into the conformational space and solvation of protein-ligand complexes. For RfaH, RfaH-rifaximin, RfaH-berberine chloride, and RfaH-(rifaximin and berberine chloride), we have generated FELs to determine energy minimum and conformational maps **(Figure 10).** The shaded deep-blue areas on the FELs correspond to low-energy conformations close to the native state. The contour maps of FELs for these complexes reveal that the binding of rifaximin and berberine chloride changes the minimum energy regions of RfaH protein. In the RfaH complex with the dual-ligand system, there is a single large, deep blue basin and a smaller basin. Whereas, in the other three systems, the basins are scattered. This indicates the stable binding of the synergistic complex with the RfaH protein.

DISCUSSION

Bacterial infections pose a growing global health threat due to antimicrobial resistance and the decline of antibiotic development pipelines, leading to increased untreatable morbidity and mortality (42, 43). Natural compounds, such as isoquinoline alkaloids, exhibit broad-spectrum antimicrobial activity and are widely distributed in nature (44). These compounds represent promising candidates against multidrug-resistant pathogens and have undergone extensive investigation (45). However, the inherent rapid evolutionary capacity of bacteria prompts the discovery of novel strategies to prevent the development of resistance. While numerous potent natural antimicrobials have entered clinical trials, their deployment, like all antibiotics, carries the inherent risk of adaptive resistance negating efficacy. A key strategy to

reduce the risk of clinical resistance involves using natural compounds in synergistic antimicrobial combinations (46). Such synergistic interactions enhance lethality, potentially lowering the probability of bacterial escape mutants and subsequent resistance evolution. This combinatorial approach focuses on identifying pairs that yield effective antimicrobial synergy to prolong the utility of compounds.

Our study demonstrates enhanced combinatorial activity between berberine chloride and rifaximin against KP. While the FICI (0.56) indicates partial synergy in static MIC assays, the time-kill data revealed an additive to moderately enhanced bactericidal effect, with the combination achieving ~0.98 $\log_{10}$ greater killing than rifaximin alone at 24 hours - a meaningful enhancement that falls short of the predefined ≥2 $\log_{10}$ threshold for time-kill synergy. Building on our prior study showing that rifaximin targets the essential anti-terminator factor RfaH in KP, molecular docking reveals that both compounds (rifaximin and berberine chloride) occupy the RfaH binding pocket and form hydrogen bonds with functionally critical residues. This dual binding is corroborated by intrinsic fluorescence quenching assays, in which a 1:1 mixture shows additive quenching of RfaH and a 10-fold increase in the association constant (K_a) relative to single agents, indicating enhanced binding affinity.

RfaH transcriptionally regulates capsule production in KP by acting as an anti-terminator at the ops site within the promoter-distal region of the cps (capsular polysaccharide) operon, enabling full-length expression of genes essential for capsule biosynthesis (47). When evaluating the repurpose potential of an existing drug, two critical parameters are its enhanced efficacy and improved specificity in the new therapeutic context. The rifaximin-berberine combination demonstrates significant advantages in both areas compared to rifaximin monotherapy. While rifaximin alone shows moderate activity, its partnership with berberine chloride dramatically enhances potency, reducing the MIC of berberine by 16-fold to 6.25 μM and that of rifaximin by 2-fold to 50 μM. This demonstrates that the combination can achieve robust therapeutic outcomes at lower, potentially safer doses of the repurposed drug. Regarding specificity, combining actions through RfaH inhibition offers a targeted anti-virulence strategy rather than a broad-spectrum bactericidal approach.

Rifaximin, in its original indication, acts locally in the gut with minimal systemic absorption. Its repurposed mechanism, as revealed here, is highly specific and directly binds to and inhibits a master regulator of virulence. By targeting RfaH, the combination specifically disarms the pathogen by suppressing capsule production, a key virulence determinant, without exerting the strong selective pressure for resistance typically associated with essential target inhibition. This dual improvement highlights a highly favorable profile for drug repurpose. This strategy offers a pragmatic and powerful approach to rapidly deploy a refined, combination-based therapy against multidrug-resistant KP, potentially extending the lifespan and utility of both an existing drug and a natural antimicrobial compound.

While this study presents a compelling case for RfaH-targeted synergy, its limitations must be acknowledged. The findings, derived from *in vitro* models using a single KP strain, require validation across diverse clinical isolates to confirm broad applicability. Furthermore, the exclusive focus on RfaH inhibition leaves unexplored the plausible contribution of off-target effects to the observed synergy.

It is important to note that the experimental work in this study was performed using *Klebsiella quasipneumoniae subsp. similipneumoniae* (ATCC 700603), a strain frequently employed as a reference in antimicrobial resistance studies. While this strain shares core genetic and pathogenic mechanisms with clinically prevalent KP isolates, particularly the conserved role of the RfaH regulator in capsule biosynthesis and virulence, extrapolating our synergistic efficacy data to diverse clinical KP strains, especially hypervirulent or carbapenem-resistant variants, requires further validation. This represents a limitation of the present *in vitro* study. Future work will prioritize evaluating the berberine-rifaximin combination against a panel of contemporary, multidrug-resistant KP clinical isolates to confirm the broad applicability of this combinatorial efficacy and its potential impact on AMR in a clinically relevant context.

Also, we must prioritize *in vivo* validation in animal models and expand testing to diverse clinical isolates. Mechanistic studies should delineate off-target effects using transcriptomics and rigorously assess the combination's ability to suppress resistance emergence. For clinical translation, developing novel formulations to overcome rifamycin's poor systemic absorption is crucial. Ultimately, this work establishes a

platform for discovering next-generation RfaH-targeted anti-virulence therapies against multidrug-resistant pathogens.

CONCLUSION

This study demonstrates that berberine chloride and rifaximin act synergistically against KP. Integrated *in silico* and biophysical data support a model wherein this synergy involves dual targeting of the transcriptional anti-terminator RfaH. Mechanistically, both compounds concurrently occupy the binding pocket, forming stabilizing interactions with key residues, as evidenced by molecular docking, intrinsic fluorescence quenching, and molecular dynamics simulations confirming ternary complex stability. Functionally, the combination achieved a 2.56 $\log_{10}$ reduction in bacterial viability from the starting inoculum and suppressed capsule production at half the rifaximin concentration required for monotherapy. These findings validate RfaH as a druggable target and support the development of combinatorial strategies to enhance antimicrobial efficacy while reducing effective doses. The repurposing of rifaximin with berberine offers a promising clinical strategy against KP by leveraging their synergistic, bactericidal action via dual RfaH inhibition. This combination could enhance treatment efficacy against multidrug-resistant strains while potentially reducing the development of resistance. The main therapeutic advantage lies in its anti-virulence mechanism, which disrupts capsule production without requiring intense selective pressure. Clinically, the established safety profile of rifaximin facilitates rapid repurposing, and this combination could become a novel, targeted therapy for resistant KP infections.

ACKNOWLEDGMENTS

AA sincerely thanks the Indian Council of Medical Research-Department of Health Research (File No. R.12014/06/2022-HR).

Conflicts of interest: Authors declare no conflicts of interest.

Funding: This work is funded and supported by the Indian Council of Medical Research (Grant No. ECD/adoc/2/2021-22).

Data availability: The data supporting the findings are available within the article and supplementary materials.

Submitted: December 20, 2025

Accepted: January 22, 2026

Published online: January 28, 2026

REFERENCES

1.Effah CY, Sun T, Liu S, Wu Y. Klebsiella pneumoniae: an increasing threat to public health. Annals of clinical microbiology and antimicrobials. 2020;19:1–9. https://doi.org/10.1186/s12941-019-0343-8

2.Douradinha B. Should multidrug resistant Klebsiella pneumoniae strains displaying hypervirulent traits be reclassified as either ultravirulent or supervirulent? Microbiol Res. 2023;275:127446. https://doi.org/10.1016/j.micres.2023.127446

3.Li L, Li S, Wei X, Lu Z, Qin X, Li M. Infection with carbapenem-resistant hypervirulent Klebsiella pneumoniae: clinical, virulence and molecular epidemiological characteristics. Antimicrobial Resistance & Infection Control. 2023;12(1):124. https://doi.org/10.1186/s13756-023-01331-y

4.Sati H, Carrara E, Savoldi A, Hansen P, Garlasco J, Campagnaro E, et al. The WHO bacterial priority pathogens list 2024: a prioritisation study to guide research, development, and public health strategies against antimicrobial resistance. The Lancet infectious diseases. 2025. https://doi.org/10.1016/S1473-3099(25)00118-5

5.Gan L, Mao P, Tian Z, Li X, Yu Z, Du B, et al. Higher prevalence of hypervirulent Klebsiella pneumoniae isolates with high-risk multidrug resistance in Asia. Journal of Infection and Public Health. 2025;18(9):102834. https://doi.org/10.1016/j.jiph.2025.102834

6.Douradinha B. Exploring the journey: a comprehensive review of vaccine development against Klebsiella pneumoniae. Microbiol Res. 2024;287:127837. https://doi.org/10.1016/j.micres.2024.127837

7.Li Y, Kumar S, Zhang L. Mechanisms of antibiotic resistance and developments in therapeutic strategies to combat Klebsiella pneumoniae infection. Infection and Drug Resistance. 2024:1107–19. https://doi.org/10.2147/IDR.S453025

8.Saeed MU, Ahmed S, Choudhury A, Hussain A, Alajmi MF, Mohammad T, et al. Discovering novel inhibitors of RfaH from Klebsiella pneumoniae to combat antimicrobial resistance. Archives of Microbiology. 2024;206(12):472. https://doi.org/10.1007/s00203-024-04192-0

9.Wu K-M, Li L-H, Yan J-J, Tsao N, Liao T-L, Tsai H-C, et al. Genome sequencing and comparative analysis of Klebsiella pneumoniae NTUH-K2044, a strain causing liver abscess and meningitis. Journal of bacteriology. 2009;191(14):4492–501. https://doi.org/10.1128/JB.00315-09

10.Tian D, Liu X, Chen W, Zhou Y, Hu D, Wang W, et al. Prevalence of hypervirulent and carbapenem-resistant Klebsiella pneumoniae under divergent evolutionary patterns. Emerging microbes & infections. 2022;11(1):1936–49. https://doi.org/10.1080/22221751.2022.2103454

11.Russo TA, Marr CM. Hypervirulent Klebsiella pneumoniae. Clinical microbiology reviews. 2019;32(3):e00001–19. https://doi.org/10.1128/CMR.00001-19

12.Bezerra dos Santos AT, Araújo TFdS, Nascimento da Silva LC, Silva CBd, Oliveira AFMd, Araújo JM, et al. Organic extracts from Indigofera suffruticosa leaves have antimicrobial and synergic actions with erythromycin against Staphylococcus aureus. Frontiers in Microbiology. 2015;6:13. https://doi.org/10.3389/fmicb.2015.00013

13.Sasidharan S, Tripathi T, Saudagar P. Critical insight into plausible acquired tocopherol pathway in neglected human trypanosomatids. ACS omega.

2021;6(47):31396–403.
https://doi.org/10.1021/acsomega.1c05046

14.Saifi S, Ashraf A, Hasan GM, Shamsi A, Hassan MI. Insights into the preventive actions of natural compounds against Klebsiella pneumoniae infections and drug resistance. Fitoterapia. 2024;173:105811.
https://doi.org/10.1016/j.fitote.2023.105811

15.Yan D, Jin C, Xiao X-H, Dong X-P. Antimicrobial properties of berberines alkaloids in Coptis chinensis Franch by microcalorimetry. Journal of biochemical and biophysical methods. 2008;70(6):845–9.
https://doi.org/10.1016/j.jbbm.2007.07.009

16.Xia S, Ma L, Wang G, Yang J, Zhang M, Wang X, et al. In vitro antimicrobial activity and the mechanism of berberine against methicillin-resistant Staphylococcus aureus isolated from bloodstream infection patients. Infection and Drug Resistance. 2022;15:1933–44.
https://doi.org/10.2147/IDR.S357077

17.Noghabi SA, Bagherzade G, Beyzaei H. Comparative study of antioxidant and antimicrobial activity of berberine-derived Schiff bases, nitro-berberine and amino-berberine. Heliyon. 2023;9(12):e22783.
https://doi.org/10.1016/j.heliyon.2023.e22783

18.Ashraf A, Choudhary A, Khan MA, Noor S, Islam A, Hassan MI. Repurposing rifaximin against Klebsiella pneumoniae via targeting of transcription anti-termination protein RfaH for novel antimicrobial development. 2024.
https://doi.org/10.21203/rs.3.rs-4724428/v1

19.Ali S, Alam M, Hasan GM, Hassan MI. Potential therapeutic targets of Klebsiella pneumoniae: a multi-omics review perspective. Brief Funct Genomics. 2022;21(2):63–77.
https://doi.org/10.1093/bfgp/elab038

20.Anwar S, Khan S, Shamsi A, Anjum F, Shafie A, Islam A, et al. Structure-based investigation of MARK4 inhibitory potential of naringenin for therapeutic

management of cancer and neurodegenerative diseases. Journal of cellular biochemistry. 2021;122(10):1445–59.
https://doi.org/10.1002/jcb.30022

21.Dahiya R, Mohammad T, Roy S, Anwar S, Gupta P, Haque A, et al. Investigation of inhibitory potential of quercetin to the pyruvate dehydrogenase kinase 3: towards implications in anticancer therapy. International journal of biological macromolecules. 2019;136:1076–85.
https://doi.org/10.1016/j.ijbiomac.2019.06.158

22.Gulzar M, Ali S, Khan FI, Khan P, Taneja P, Hassan MI. Binding mechanism of caffeic acid and simvastatin to the integrin linked kinase for therapeutic implications: a comparative docking and MD simulation studies. Journal of Biomolecular Structure and Dynamics. 2019;37(16):4327–37.
https://doi.org/10.1080/07391102.2018.1546621

23.Kowalska-Krochmal B, Dudek-Wicher R. The minimum inhibitory concentration of antibiotics: methods, interpretation, clinical relevance. Pathogens. 2021;10:165.
https://doi.org/10.3390/pathogens10020165

24.Rodríguez-Melcón C, Alonso-Calleja C, García-Fernández C, Carballo J, Capita R. Minimum inhibitory concentration (MIC) and minimum bactericidal concentration (MBC) for twelve antimicrobials (biocides and antibiotics) in eight strains of Listeria monocytogenes. Biology. 2021;11(1):46.
https://doi.org/10.3390/biology11010046

25.Petersen PJ, Labthavikul P, Jones CH, Bradford PA. In vitro antibacterial activities of tigecycline in combination with other antimicrobial agents determined by chequerboard and time-kill kinetic analysis. Journal of Antimicrobial Chemotherapy. 2006;57(3):573–6.
https://doi.org/10.1093/jac/dki477

26.Blumenkrantz N, Asboe-Hansen G. New method for quantitative determination of uronic acids. Analytical biochemistry. 1973;54(2):484–9.
https://doi.org/10.1016/0003-2697(73)90377-1

27.Lin T-L, Yang F-L, Yang A-S, Peng H-P, Li T-L, Tsai M-D, et al. Amino acid substitutions of MagA in Klebsiella pneumoniae affect the biosynthesis of the capsular polysaccharide. PLoS One. 2012;7(10):e46783.
https://doi.org/10.1371/journal.pone.0046783

28.Svetlov D, Shi D, Twentyman J, Nedialkov Y, Rosen DA, Abagyan R, et al. In silico discovery of small molecules that inhibit RfaH recruitment to RNA polymerase. Molecular microbiology. 2018;110(1):128–42.
https://doi.org/10.1111/mmi.14093

29.Mohammad T, Mathur Y, Hassan MI. InstaDock: a single-click graphical user interface for molecular docking-based virtual high-throughput screening. Briefings in Bioinformatics. 2021;22(4):bbaa279.
https://doi.org/10.1093/bib/bbaa279

30.DeLano WL. Pymol: an open-source molecular graphics tool. CCP4 Newsl protein crystallogr. 2002;40(1):82–92.

31.Hassan MI, Anjum D, Mohammad T, Alam M, Khan MS, Shahwan M, et al. Integrated virtual screening and MD simulation study to discover potential inhibitors of Lyn-kinase: targeting cancer therapy. J Biomol Struct Dyn. 2022:1–11.
https://doi.org/10.1080/07391102.2022.2154849

32.Jairajpuri DS, Mohammad T, Adhikari K, Gupta P, Hasan GM, Alajmi MF, et al. Identification of sphingosine kinase-1 inhibitors from bioactive natural products targeting cancer therapy. ACS Omega. 2020;5(24):14720–9.
https://doi.org/10.1021/acsomega.0c01511

33.Van Der Spoel D, Lindahl E, Hess B, Groenhof G, Mark AE, Berendsen HJ. GROMACS: fast, flexible, and free. Journal of computational chemistry. 2005;26(16):1701–18.
https://doi.org/10.1002/jcc.20291

34.Huang J, MacKerell Jr AD. CHARMM36 all-atom additive protein force field: validation based on comparison to NMR data. Journal of computational chemistry.

2013;34(25):2135–45.
https://doi.org/10.1002/jcc.23354

35.Cai Q, Yang M, Liu D, Chen J, Shu D, Xia J, et al. Experimental treatment with favipiravir for COVID-19: an open-label control study. Engineering. 2020;6(10):1192–8.
https://doi.org/10.1016/j.eng.2020.03.007

36.Bansal KK, Goyal R, Sharma A, Sharma PC, Goyal RK. Repurposing of drugs for the treatment of microbial diseases. Drug Repurposing for Emerging Infectious Diseases and Cancer. 2023:347–94.
https://doi.org/10.1007/978-981-19-5399-6_16

37.Kang JY, Mooney RA, Nedialkov Y, Saba J, Mishanina TV, Artsimovitch I, et al. Structural basis for transcript elongation control by NusG family universal regulators. Cell. 2018;173(7):1650–62.e14.
https://doi.org/10.1016/j.cell.2018.05.017

38.Galaz-Davison P, Román EA, Ramírez-Sarmiento CA. The N-terminal domain of RfaH plays an active role in protein fold-switching. PLoS computational biology. 2021;17(9):e1008882.
https://doi.org/10.1371/journal.pcbi.1008882

39.Bulusu G, Desiraju GR. Strong and weak hydrogen bonds in protein-ligand recognition. Journal of the Indian Institute of Science. 2020;100(1):31–41.
https://doi.org/10.1007/s41745-019-00141-9

40.de Brevern AG. Impact of protein dynamics on secondary structure prediction. Biochimie. 2020;179:14–22.
https://doi.org/10.1016/j.biochi.2020.09.006

41.Moradi S, Nowroozi A, Nezhad MA, Jalali P, Khosravi R, Shahlaei M. A review on description dynamics and conformational changes of proteins using combination of principal component analysis and molecular dynamics simulation. Computers in Biology and Medicine. 2024;183:109245.
https://doi.org/10.1016/j.compbiomed.2024.109245

42.Larsson D, Gaze W, Laxminarayan R, Topp E. AMR, One Health and the environment. Nature Microbiology. 2023;8(5):754–5.
https://doi.org/10.1038/s41564-023-01351-9

43.Padhi AK, Tripathi T. A comprehensive protein design protocol to identify resistance mutations and signatures of adaptation in pathogens. Briefings in Functional Genomics. 2023;22(2):195–203.
https://doi.org/10.1093/bfgp/elac020

44.Shukla R, Shukla H, Tripathi T. Structural and energetic understanding of novel natural inhibitors of Mycobacterium tuberculosis malate synthase. Journal of Cellular Biochemistry. 2019;120(2):2469–82.
https://doi.org/10.1002/jcb.27538

45.Yang M, Dong M, Wu Q-Y, Yao S, Pu G, Ma Y-Y, et al. Three new isoquinoline alkaloids from the fermentation of Aspergillus sp. 0338 and their anti-MRSA activities. Natural Product Research. 2025;39(1):103–9.
https://doi.org/10.1080/14786419.2023.2254455

46.Ju J, Xie Y, Yu H, Guo Y, Cheng Y, Qian H, et al. Synergistic interactions of plant essential oils with antimicrobial agents: a new antimicrobial therapy. Critical Reviews in Food Science and Nutrition. 2022;62(7):1740–51.
https://doi.org/10.1080/10408398.2020.1846494

47.Xu L, Li J, Wu W, Wu X, Ren J. Klebsiella pneumoniae capsular polysaccharide: mechanism in regulation of synthesis, virulence, and pathogenicity. Virulence. 2024;15(1):2439509.
https://doi.org/10.1080/21505594.2024.2439509

TABLES AND FIGURES WITH LEGENDS

Table 1. Binding constants for berberine chloride, rifaximin, and their combination

S. No.	**Compound name**	Binding constant (K_a) Value
1	Berberine Chloride	1.09 X 10^6 M^{-1}
2	Rifaximin	7.38 X 10^6 M^{-1}
3	Berberine chloride + Rifaximin	6.86 X10^7 M^{-1}

Table 2. Average values of structural integrity parameters for RfaH during molecular dynamics simulations in both unbound and bound states at 310 K

System	**RMSD (nm)**	**RMSF (nm)**	***R*g (nm)**	**SASA (nm^2)**	**#H-bonds**
RfaH	0.41	0.24	1.78	109.64	98
RfaH-Berberine	0.57	0.28	1.79	113.92	96
RfaH-Rifaximin	0.67	0.30	1.75	114.12	98
RfaH-(Berberine+Rifaximin)	0.36	0.21	1.79	110.95	99

Abbreviations: RMSD: Root mean square deviation; RMSF: Root mean square fluctuation; Rg: Radius of gyration; SASA: Solvent-accessible surface area; H-bonds: Hydrogen bonds

Table 3. Residue counts in the secondary structures of RfaH in both unbound and various bound forms at 310 K

	RfaH	**RfaH-berberine**	**RfaH-rifaximin**	**RfaH-(berberine+rifaximin)**
Coil	33	31	32	33
β-sheet	36	34	36	36
β-bridge	1	2	0	1
Bend	16	16	15	14
Turn	20	19	17	19
α-helix	51	53	55	53
π-helix	0	0	0	0
3_{10}-helix	0	1	1	1
κ-Helix	5	6	6	5

Abbreviation: RfaH: Transcriptional antitermination factor RfaH.

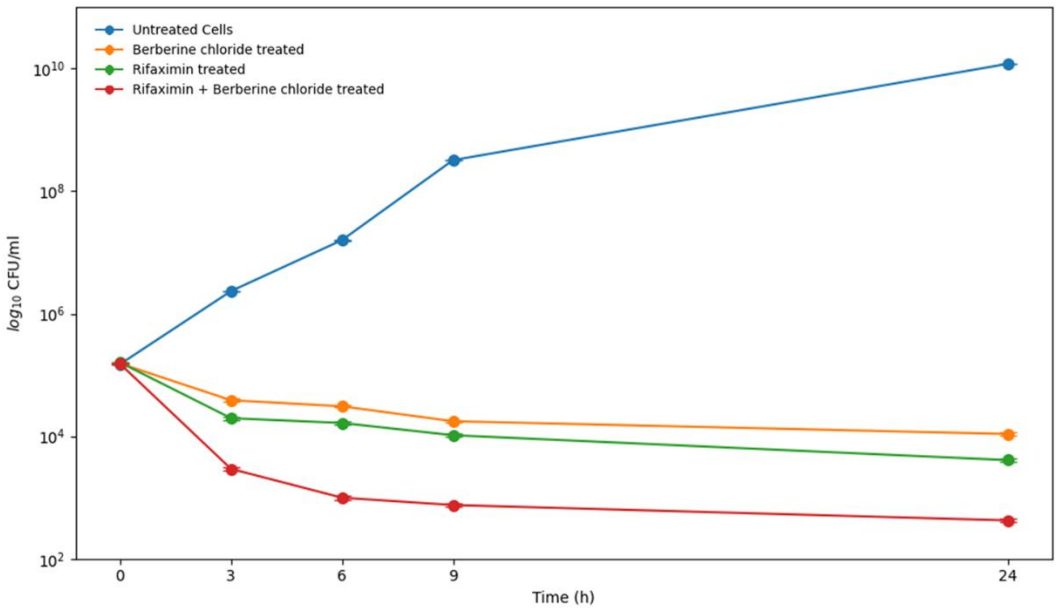

Figure 1. Time–kill kinetics of KP ATCC 700603 following rifaximin and berberine chloride monotherapy or combination treatment. Early log-phase cultures (starting inoculum ≈1.5 × 10^5 CFU/mL) were exposed to rifaximin (100 µM), berberine chloride (100 µM), or the synergistic checkerboard-derived combination (50 µM rifaximin + 6.25 µM berberine chloride), alongside an untreated growth control, and viable counts were quantified over 24 h by colony enumeration. The combination produced enhanced killing relative to either single agent, achieving a 2.56 log_{10} CFU/mL reduction from baseline at 24 h versus 1.59 log_{10} for rifaximin alone (Δ ≈0.98 log_{10}). This improvement did not meet the predefined time–kill synergy criterion (≥2 log_{10} CFU/mL decrease compared with the most active single agent at the same time point). Data are mean log_{10} CFU/mL ± SD from three independent experiments. **Abbreviations**: KP: *Klebsiella pneumoniae*; ATCC: American Type Culture Collection; CFU: colony-forming unit; SD: standard deviation.

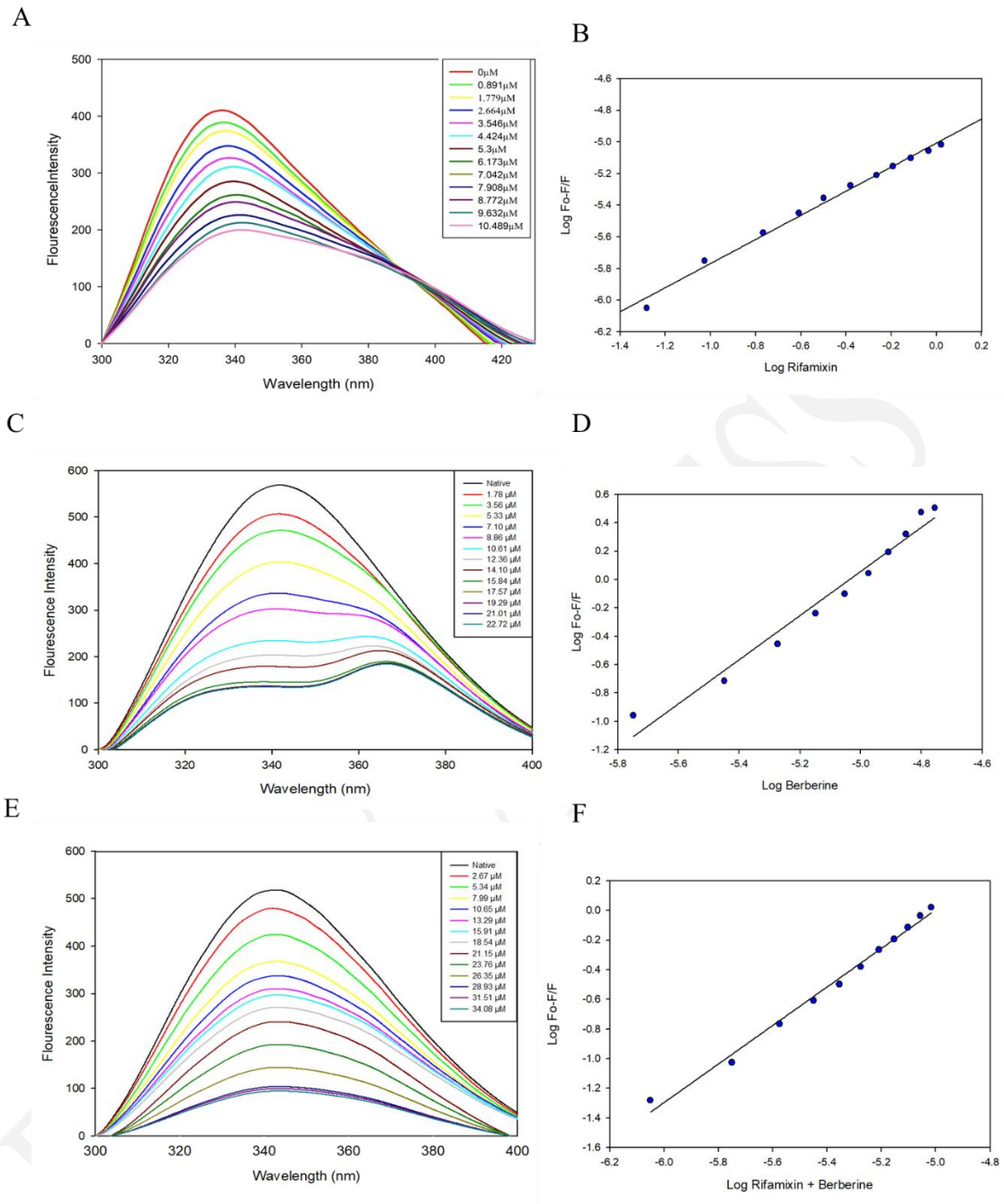

Figure 2. Intrinsic fluorescence quenching of RfaH by rifaximin, berberine chloride, and their combination. (A, C, E) Emission spectra of RfaH recorded upon titration with increasing concentrations of rifaximin, berberine chloride, or an 8:1 (rifaximin:berberine chloride) mixture. Samples were excited at 280 nm and emission was collected from 300–400 nm. Progressive quenching with increasing ligand concentration indicates direct ligand engagement with RfaH. The 8:1 mixture produced a stronger quenching response consistent with cooperative binding. **(B, D, F)**

Modified Stern–Volmer analyses of the corresponding titrations used to estimate Ka. Rifaximin bound RfaH with high affinity ($K_a = 7.38 \times 10^6\ M^{-1}$), berberine chloride exhibited moderate affinity ($K_a = 1.09 \times 10^6\ M^{-1}$), and the 8:1 mixture yielded a markedly enhanced affinity ($K_a = 6.86 \times 10^7\ M^{-1}$), indicating synergistically strengthened binding. **Abbreviation**: RfaH: transcriptional antitermination factor.

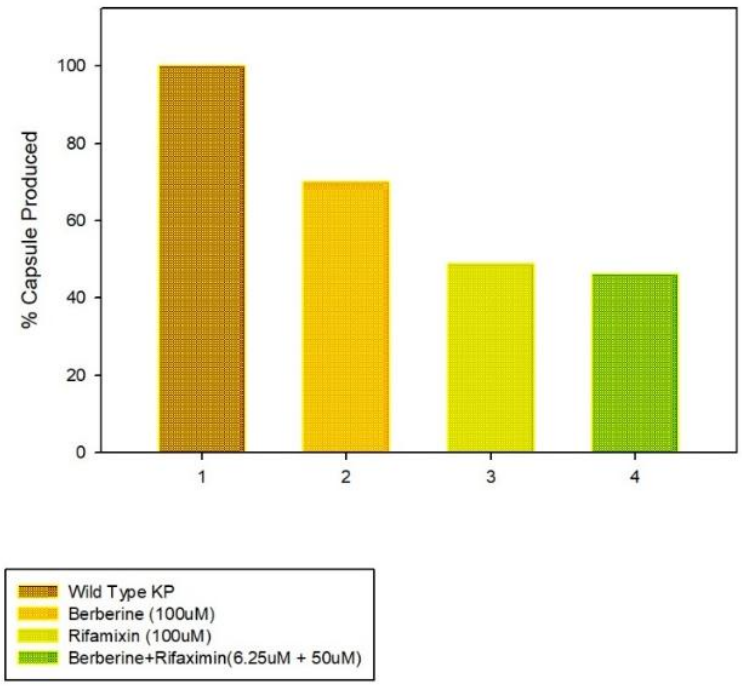

Figure 3. CPS production in KP following treatment with rifaximin, berberine chloride, or rifaximin+berberine chloride. CPS levels were quantified in KP after 16 h exposure to rifaximin (100 µM), berberine chloride (100 µM), or rifaximin+berberine chloride (50 µM + 6.25 µM). CPS is expressed as % capsule produced relative to the untreated control (set to 100%) after normalization to CFU/mL. Rifaximin alone reduced CPS by >50%, berberine chloride produced a more modest reduction (~30%), and rifaximin+berberine chloride achieved CPS suppression comparable to rifaximin monotherapy despite a 2-fold lower rifaximin concentration. Data are representative of three independent experiments with consistent trends. **Abbreviations**: CPS: capsular polysaccharide; KP: *Klebsiella pneumoniae*; CFU: colony-forming unit.

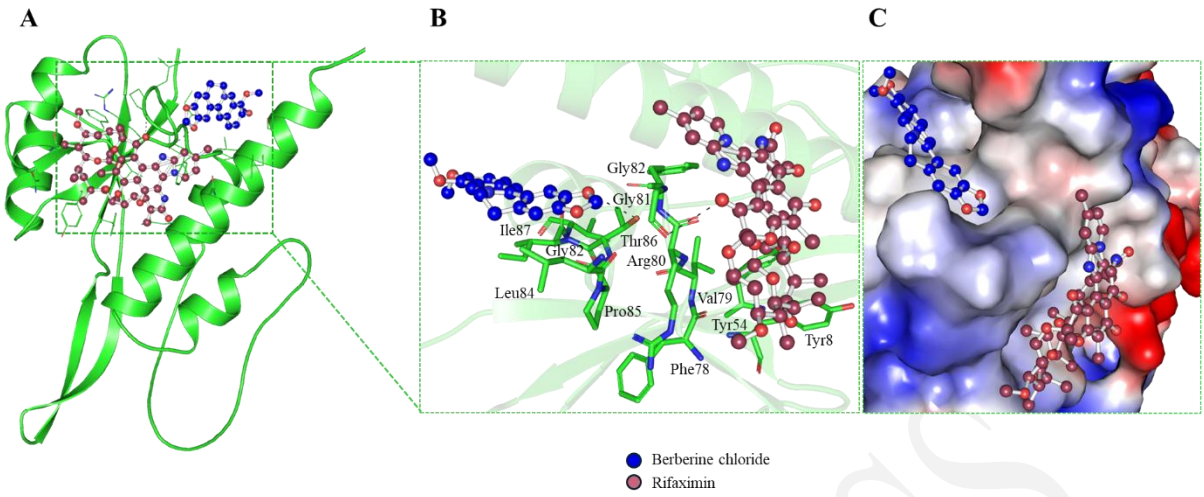

Figure 4. Docking-predicted interactions of rifaximin and berberine chloride with RfaH. (A) 2D interaction maps summarizing polar and hydrophobic contacts formed by rifaximin and berberine chloride within the RfaH binding region. **(B)** 3D binding poses highlighting key H-bonds with functionally relevant residues. Rifaximin engages the pocket via multiple stabilizing contacts, including an H-bond network involving Tyr54, consistent with inhibition at a critical functional interface. berberine chloride preferentially occupies the NTD hydrophobic patch cavity and forms H-bonds with Gly81 (3.3 Å) and Thr86 (3.5 Å), a region implicated in regulating the NTD–βCTD autoinhibitory interface and post-TEC refolding; binding at this site is therefore predicted to perturb conformational switching and dysregulate RfaH activity. **(C)** Surface representation of RfaH illustrating pocket shape complementarity and deep ligand accommodation for both rifaximin and berberine chloride. **Abbreviations**: RfaH: transcriptional antitermination factor RfaH; NTD: N-terminal domain; βCTD: beta C-terminal domain; TEC: transcription elongation complex; H-bonds: hydrogen bonds; Å: ångström.

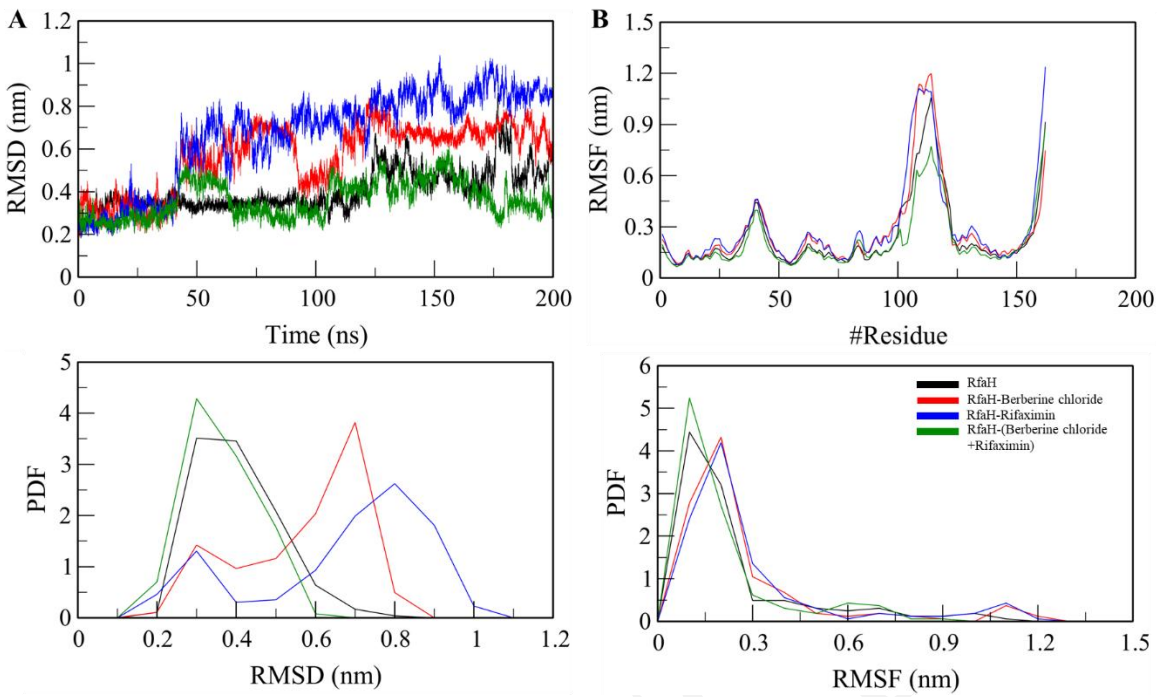

Figure 5. RMSD and RMSF profiles of RfaH during 200 ns MD simulations in apo and ligand-bound states. (A) RMSD time-evolution for apo RfaH and RfaH complexes with single ligands (rifaximin or berberine chloride) or the dual-ligand system (rifaximin+berberine chloride). Relative to apo RfaH (avg RMSD = 0.41 nm), single-ligand binding increased structural deviation (rifaximin: 0.57 nm; berberine chloride: 0.67 nm), whereas dual-ligand binding reduced RMSD (0.36 nm), indicating restoration of near-apo-like stability. The lower-left panel shows the RMSD PDF, illustrating a narrower distribution for the dual-ligand complex compared with single-ligand complexes. **(B)** Per-residue RMSF for apo and ligand-bound systems. Compared with apo RfaH (avg RMSF = 0.24 nm), residue-level flexibility increased with single ligands (rifaximin: 0.30 nm; berberine chloride: 0.28 nm) but decreased in the dual-ligand complex (0.21 nm), consistent with ligand-cooperative stabilization without major perturbation of the overall flexibility pattern. The lower-right panel shows the RMSF PDF for each system. **Abbreviations:** RMSD: root mean square deviation; RMSF: root mean square fluctuation; MD: molecular dynamics; apo: unbound; RfaH: transcriptional antitermination factor RfaH; PDF: probability density function.

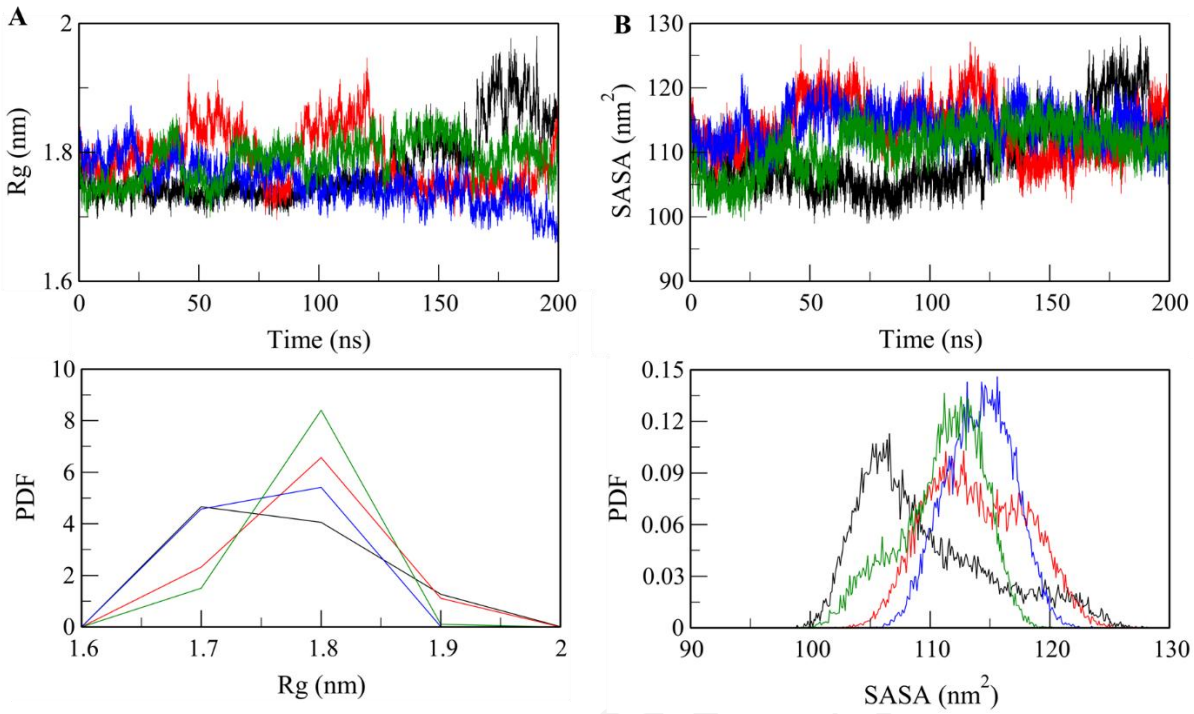

Figure 6. Rg and SASA profiles of RfaH during 200 ns MD simulations in apo and ligand-bound states. (A) Rg time-evolution for apo RfaH and RfaH complexes with rifaximin, berberine chloride, or rifaximin+berberine chloride. Mean Rg values were highly similar across systems (apo: 1.78 nm; rifaximin: 1.79 nm; berberine chloride: 1.79 nm; rifaximin+berberine chloride: 1.79 nm), indicating that ligand binding does not measurably alter global compactness. The lower-left panel shows the Rg PDF for each trajectory. **(B)** SASA time-evolution showing that single-ligand binding increased solvent exposure relative to apo RfaH (apo: 109.64 nm²; rifaximin: 114.12 nm²; berberine chloride: 113.92 nm²), whereas the dual-ligand complex shifted SASA toward the apo-like state (rifaximin+berberine chloride: 110.95 nm²), consistent with reduced structural perturbation under cooperative binding. The lower-right panel shows the SASA PDF for each trajectory. **Abbreviations:** Rg: radius of gyration; SASA: solvent-accessible surface area; MD: molecular dynamics; apo: unbound; RfaH: transcriptional antitermination factor RfaH; PDF: probability density function.

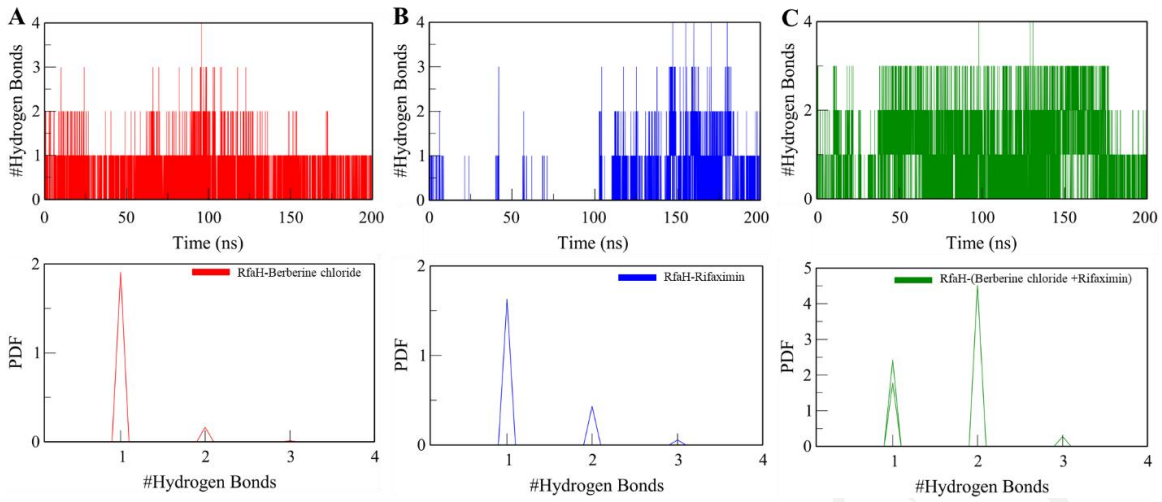

Figure 7. Intermolecular H-bonding between RfaH and ligands during 200 ns MD simulations. (A–C) Time-resolved counts of intermolecular H-bonds formed between RfaH and **(A)** berberine chloride, **(B)** rifaximin, or **(C)** the dual-ligand system (rifaximin+berberine chloride). Both single-ligand complexes formed up to 4 H-bonds, with an average occupancy centered at ~1 H-bond over the trajectory; the berberine chloride complex retained ~1 persistent H-bond. In contrast, the dual-ligand complex also reached up to 4 H-bonds but maintained ~2 persistent H-bonds across the simulation, consistent with enhanced and more sustained intermolecular stabilization. (Lower panels) PDFs of H-bond counts show the dominant population at 1 H-bond for the single-ligand complexes, whereas the dual-ligand complex exhibits its main peak at 2 H-bonds, supporting increased H-bond occupancy under cooperative binding. **Abbreviations:** H-bond: hydrogen bond; MD: molecular dynamics; RfaH: transcriptional antitermination factor RfaH; PDF: probability density function.

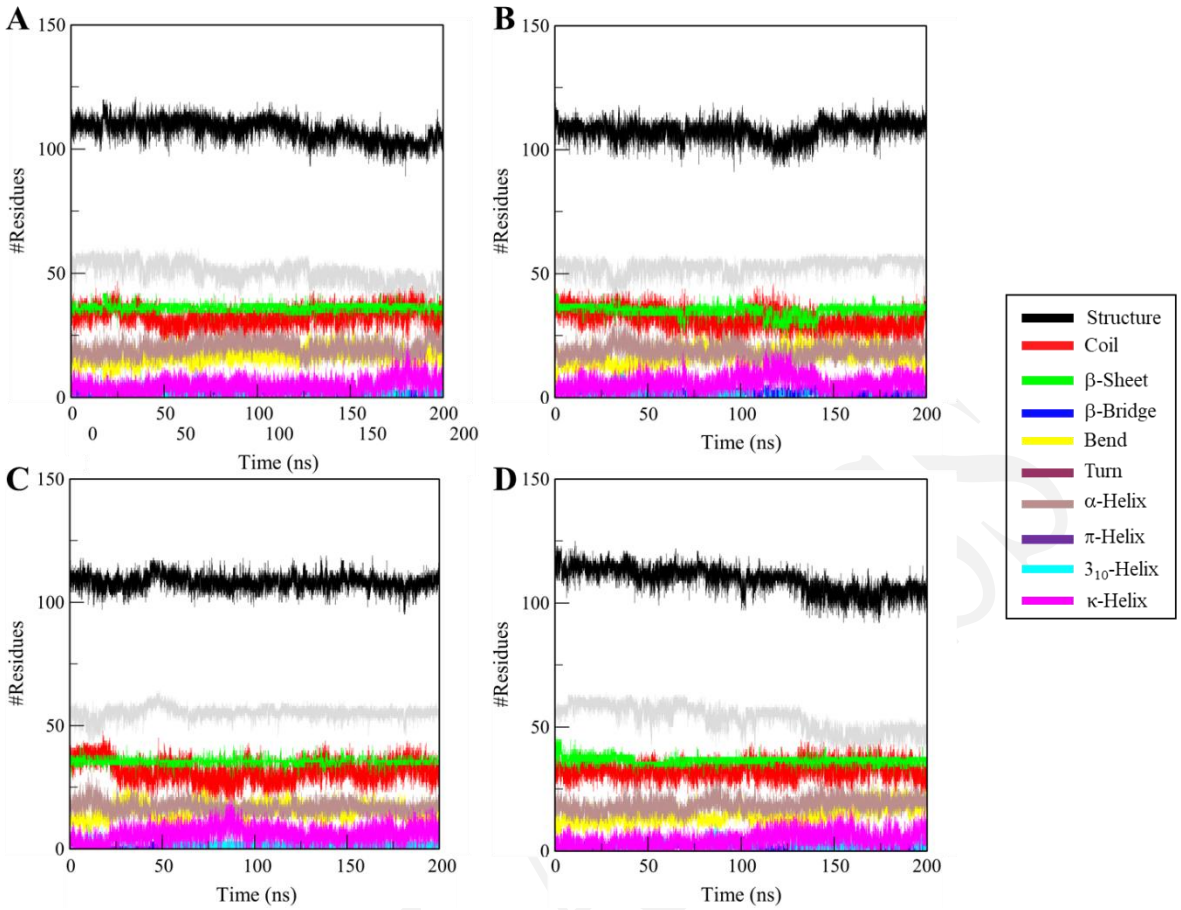

Figure 8. Secondary-structure time evolution of RfaH during 200 ns MD simulations in apo and ligand-bound states. (A–D) Secondary-structure assignments plotted as residue counts versus time for **(A)** apo RfaH, **(B)** RfaH–rifaximin, **(C)** RfaH–berberine chloride, and **(D)** RfaH–rifaximin+berberine chloride. Across all trajectories, the secondary-structure topology remained stable, with no evidence of global unfolding. The RfaH–rifaximin and RfaH–berberine chloride complexes largely preserved the apo-like α/β architecture, indicating that single-ligand binding does not destabilize the fold. The RfaH–rifaximin+berberine chloride system exhibited subtle, cooperative remodeling consistent with a minor reduction in β-structure accompanied by a modest increase in α-helical content, while retaining the overall native-like secondary-structure framework. **Abbreviations:** MD: molecular dynamics; apo: unbound; RfaH: transcriptional antitermination factor RfaH.

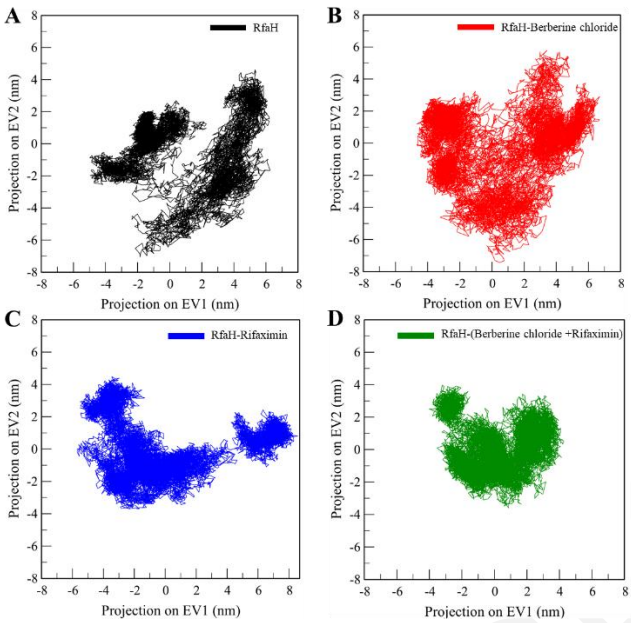

Figure 9. PCA projections of RfaH conformational sampling during MD simulations. (A–D) 2D projections of MD trajectories onto the first two principal components (EV1 and EV2), computed from Cα coordinates for **(A)** apo RfaH, **(B)** RfaH–berberine chloride, **(C)** RfaH–rifaximin, and **(D)** RfaH–rifaximin+berberine chloride. Single-ligand complexes explored conformational space comparable to, or broader than, apo RfaH, whereas the dual-ligand system occupied a markedly more confined subspace, indicating restricted collective motions and enhanced conformational stabilization of RfaH under cooperative binding. **Abbreviations:** PCA: principal component analysis; MD: molecular dynamics; EV1/EV2: eigenvector 1/2 (principal components 1/2); Cα: alpha carbon; apo: unbound; RfaH: transcriptional antitermination factor RfaH.

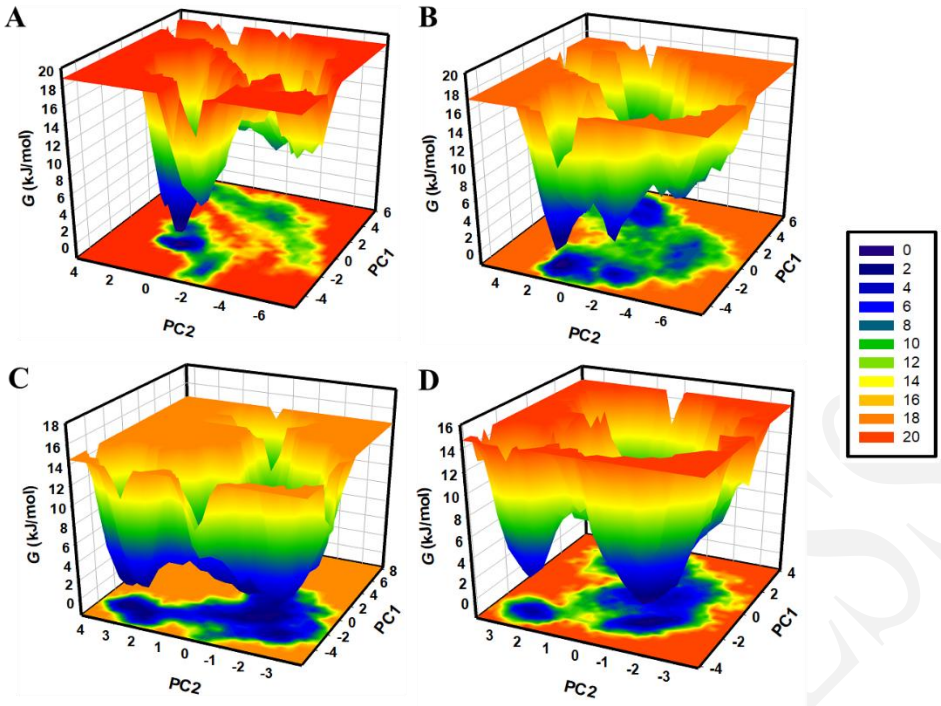

Figure 10. FELs of RfaH conformational states derived from MD trajectories. **(A–D)** FELs mapped onto PC1 and PC2 for **(A)** apo RfaH, **(B)** RfaH–berberine chloride, **(C)** RfaH–rifaximin, and **(D)** RfaH–rifaximin+berberine chloride. Color gradients denote relative free energy (G), with deep-blue regions representing low-energy conformations. Apo RfaH and single-ligand systems exhibit multiple, dispersed minima, consistent with broader conformational sampling and heterogeneous low-energy states. In contrast, the dual-ligand system displays a dominant, deep-blue basin with a secondary smaller basin, indicating a more focused low-energy ensemble and increased conformational stabilization of RfaH under cooperative binding. **Abbreviations:** FEL: free energy landscape; MD: molecular dynamics; PC1/PC2: principal component 1/2; G: Gibbs free energy; apo: unbound; RfaH: transcriptional antitermination factor RfaH.

SUPPLEMENTAL DATA

Supplementary table 1. Results of the checkerboard assay for rifaximin and berberine chloride against KP ATCC 700603

Rifaximin (µM) ↓ Berberine (µM) →	100	50	25	12.5	6.25	3.125	1.56	0.78
100	−	−	−	−	−	+	+	+
50	−	−	−	−	MIC Combo	+	+	+
25	−	−	−	+	+	+	+	+
12.5	−	−	+	+	+	+	+	+
6.25	−	+	+	+	+	+	+	+
3.125	+	+	+	+	+	+	+	+

Note: Growth: +; No Growth: −. **Abbreviation**: MIC: minimum inhibitory concentration.

Supplementary table 2. Time-kill kinetics of rifaximin, berberine chloride, and their combination against KP (atcc 700603)

Time (Hr)	Replicate	Control	Berberine (100 µM)	Rifaximin (100 µM)	Combination (50 µM Rif + 6.25 µM Ber)
0.0	1	5.176	5.188	5.204	5.182
	2	5.172	5.182	5.199	5.178
	3	5.180	5.193	5.210	5.186
Mean ± SD	**5.176 ± 0.004**	**5.188 ± 0.006**	**5.204 ± 0.005**	**5.182 ± 0.004**	
3.0	1	6.369	4.588	4.295	3.467
	2	6.364	4.562	4.267	3.439
	3	6.375	4.612	4.320	3.493
Mean	**6.369 ±**	**4.587 ±**	**4.294 ±**	**3.466 ± 0.027**	

± SD	**0.006**	**0.025**	**0.026**		
6.0	1	7.201	4.489	4.216	2.997
	2	7.196	4.470	4.190	2.964
	3	7.207	4.506	4.241	3.028
Mean ± SD	**7.201 ± 0.006**	**4.488 ± 0.018**	**4.216 ± 0.026**	**2.996 ± 0.032**	
9.0	1	8.507	4.245	4.017	2.877
	2	8.502	4.225	3.991	2.851
	3	8.511	4.263	4.040	2.901
Mean ± SD	**8.507 ± 0.005**	**4.244 ± 0.019**	**4.016 ± 0.025**	**2.876 ± 0.025**	
24.0	1	10.079	4.037	3.610	2.626
	2	10.072	4.009	3.586	2.600
	3	10.086	4.064	3.633	2.651
Mean ± SD	**10.079 ± 0.007**	**4.036 ± 0.028**	**3.610 ± 0.024**	**2.626 ± 0.026**	

Note: Data are presented as mean ± standard deviation (SD) from three independent experiments ($n = 3$). The term "Rif+Ber" refers to the combination of rifaximin (50 μM) and berberine chloride (6.25 μM). The starting inoculum was approximately 5.18 $\log_{10}$ CFU/mL. The results indicate that rifaximin resulted in a 1.594 $\log_{10}$ reduction in viable counts (5.204 – 3.610), while the combination treatment achieved a 2.556 $\log_{10}$ reduction (5.182 – 2.626). **Abbreviations**: KP: *Klebsiella pneumoniae*; ATCC: American Type Culture Collection; Rif: rifaximin; Ber: berberine chloride; SD: standard deviation.